Virology 533 (2019) 59–67

Contents lists available at ScienceDirect

Virology

journal homepage: www.elsevier.com/locate/virology

Comparative analysis of viral entry for Asian and African lineages of Zika virus

Nicholas Rinkenberger, John W. Schoggins*

Department of Microbiology, University of Texas Southwestern Medical Center, Dallas, TX, 75390, USA

ARTICLE INFO

Keywords:
Zika
Flavivirus
Entry
Internalization
Endosome

ABSTRACT

Zika virus (ZIKV) is an emerging pathogen with global health and economic impacts. ZIKV circulates as two major lineages, Asian or African. The Asian lineage has recently been associated with significant disease in humans. Numerous studies have revealed differences between African and Asian ZIKV strains with respect to cellular infectivity, pathogenesis, and immune activation. Less is known about the mechanism of ZIKV entry and whether viral entry differs between strains. Here, we characterized ZIKV entry with two Asian and two African strains. All viruses exhibited a requirement for clathrin-mediated endocytosis and Rab5a function. Additionally, all ZIKV strains tested were sensitive to pH in the range of 6.5–6.1 and were reliant on endosomal acidification for infection. Finally, we provide direct evidence that ZIKV primarily fuses with late endosomes. These findings contribute new insight into the ZIKV entry process and suggest that divergent ZIKV strains enter cells in a highly conserved manner.

1. Introduction

Zika virus (ZIKV) is an emerging arbovirus of the *Flaviviridae* family which has caused recent outbreaks in the Yap Islands (2007), Pacific Islands (2013–2015), and the Americas (2015–2017). ZIKV infection has most notably been associated with microcephaly and ocular abnormalities in newborns and Guillain-Barre syndrome in adults (Hills et al., 2017; Ventura and Ventura, 2018). ZIKV was first identified in Uganda in 1947, and has been known to circulate in both Africa and Asia since the 1960s (Beaver et al., 2018). Sequencing and phylogenetic analysis of ZIKV isolates from recent outbreaks identified these strains as originating from the Asian lineage of ZIKV (Zhu et al., 2016; Enfissi et al., 2016; Lanciotti et al., 2016; Haddow et al., 2012; Faye et al., 2014). Intriguingly, only very rare cases of infection have been associated with African lineage ZIKV. Therefore, studying the striking difference in neurovirulence observed between the two lineages of ZIKV may help to elucidate important elements of ZIKV infection in humans and associated neurological disorders.

Phylogenetic analysis of ZIKV strains has identified a number of amino acid substitutions. Comparison of African and Asian lineage ZIKV strains revealed 75 amino acid substitutions. Interestingly, 24 amino acid changes were discovered in post-epidemic Asian lineage ZIKV strains when compared to pre-epidemic strains (Zhu et al., 2016). While amino acid substitutions were identified throughout the viral genome, a concentration of amino acid substitutions was observed in the precursor membrane (prM) and envelope (E) structural genes important for viral attachment and entry (Zhu et al., 2016). Similar phylogenetic analyses have also identified high variability in the prM gene of African and Asian lineage ZIKV (Wang et al., 2016; Faria et al., 2016).

This enrichment of mutations in genes encoding structural proteins in epidemic strains of ZIKV suggests that alterations in the function or antigenic profile of these proteins may be important for virulence and pathogenicity. In agreement with this hypothesis, a recent study reported a mutation present in the prM protein of an epidemic ZIKV strain that increased neurovirulence in neonatal mice (Yuan et al., 2017). In addition, significant differences in viral infection rates, induction of apoptosis, and host response to infection have been observed between African and Asian lineage ZIKV *in vivo* and *in vitro* (Anfasa et al., 2017; Simonin et al., 2016; Zhang et al., 2016; Lazear et al., 2016; Smith et al., 2018). A recent study suggested that the *in vitro* phenotype is due in part to differences in the structural proteins of African and Asian lineage ZIKV strains (Bos et al., 2018).

Flaviviruses are enveloped viruses that generally enter cells via clathrin-mediated endocytosis. After endocytosis, these viruses fuse with specific endosomal compartments in a pH-dependent manner to release the genome into the cytoplasm (Laureti et al., 2018; van der Schaar et al., 2008a, 2008b; Kalia et al., 2013a; Chu and Ng, 2004; Schalich et al., 1996). Previous work with individual ZIKV strains has

* Corresponding author.
E-mail address: john.schoggins@utsouthwestern.edu (J.W. Schoggins).

https://doi.org/10.1016/j.virol.2019.04.008
Received 25 March 2019; Received in revised form 20 April 2019; Accepted 22 April 2019
Available online 25 April 2019
0042-6822/

shown that infection is dependent on clathrin and Rab5 function, but not Rab7 (Meertens et al., 2017; Savidis et al., 2016). Additionally, African lineage ZIKV strains have been shown to be dependent on endosomal pH as determined with lysosomotropic agents and experiments with liposomes (Persaud et al., 2018; Rawle et al., 2018). However, the endosomal population with which ZIKV fuses has not been determined. The African lineage ZIKV strain MR 766 has been frequently used to study ZIKV entry and infection (Savidis et al., 2016; Persaud et al., 2018; Muller et al., 2016). It is important to note that MR 766 has been passaged extensively in tissue culture. In this study, we characterized general features of ZIKV entry and compared African and Asian strains. We included MR 766 in this comparison to determine if extensive passage in tissue culture has altered its mode of cell entry relative to other ZIKV strains. All strains of ZIKV tested required endosomal acidification, clathrin-mediated endocytosis, and Rab5 for infection. Using viruses with fluorophore-labelled envelopes, we provide the first direct identification of the endosomal populations with which ZIKV fuses.

2. Results

2.1. African and Asian lineage Zika virus strains enter cells in a pH-dependent manner

Enveloped viruses either fuse directly with the plasma membrane or are endocytosed and fuse with an endosomal compartment to enter the cytoplasm. Flaviviruses are canonically endocytosed through clathrin-mediated endocytosis and are subsequently released into the cytoplasm from an endosomal compartment (Savidis et al., 2016; Persaud et al., 2018; Muller et al., 2016). Previous studies with African lineage ZIKV strains have suggested a similar entry pathway for African lineage ZIKV (Meertens et al., 2017; Savidis et al., 2016; Persaud et al., 2018; Rawle et al., 2018). Certain endocytosed viruses require an acidic environment for efficient fusion with host membranes. African lineage ZIKV strains are sensitive to environmental pH as well as perturbation of endosomal pH by lysosomotropic agents such as Bafilomycin A1 (BafA1), chloroquine, and ammonium chloride (NH_4Cl) (Persaud et al., 2018; Rawle et al., 2018; Muller et al., 2016). To determine if Asian and African lineage ZIKV have differential sensitivity to endosomal pH, we infected human hepatoma cell line Huh7.5 with two Asian lineage ZIKV strains (PRVABC59, PB-81) and two African lineage ZIKV strains (MR 766, DAKAR 41519) in the presence of NH_4Cl and BafA1. Cells were treated with relatively low concentrations of NH_4Cl since higher concentrations resulted in significant cell death (data not shown). All ZIKV strains tested responded similarly to both treatments (Fig. 1A, Supp. Figure 1A). ZIKV infection trended towards a reduction with NH_4Cl treatment and was highly impaired by BafA1 treatment. The dependence of ZIKV infection on endosomal pH suggests that ZIKV is endocytosed during cell entry. Additionally, since this result suggested that dependence on endosomal acidification is conserved between ZIKV lineages, we further wanted to characterize the pH sensitivity of ZIKV. The exposed surface proteins of certain endocytosed viruses, including flaviviruses, undergo pH-dependent conformational changes resulting in fusion peptide exposure and burial in eukaryotic cell membranes (Daniels et al., 1985; Stiasny et al., 2011; Sánchez-San Martín et al., 2009; Helenius et al., 1980; White and Whittaker, 2016). This process is often irreversible (Schalich et al., 1996; Daniels et al., 1985; Allison et al., 1995; Korte et al., 1999; Muller et al., 2016). Thus, exposure of virions to low pH in the absence of a target cell membrane results in loss of infectivity due to premature conformational changes in the virion and fusion peptide exposure. To determine the pH sensitivity of ZIKV in more detail, we incubated African and Asian lineage ZIKV strains in buffers ranging from pH 7.0–4.4 in increments of 0.2 pH units and assessed ZIKV infectivity. As a control, the acidic pH was neutralized with HEPES buffer before incubation with virus. Both Asian lineage ZIKV strains were affected equally by pH treatment, with half-maximal inactivation of PRVABC59 at pH 6.29 ± 0.064 and PB-81 at pH 6.29 ± 0.065 (Fig. 1B, Supp. Figure 1B). The African lineage ZIKV strain DAKAR 41519 was similarly affected, with half-maximal loss of infectivity at pH 6.15 ± 0.14. However, half-maximal inactivation for MR 766 was significantly different when compared to DAKAR 41519, occurring at pH 6.58 ± 0.22. For all ZIKV strains except MR 766, we noticed that infection was primed by mild viral pre-acidification as has been previously observed with influenza A virus (Stauffer et al., 2014). A similar phenotype has also been reported for MR 766 when incubated in a mildly basic solution prior to infection (Schalich et al., 1996; Daniels et al., 1985; Allison et al., 1995; Korte et al., 1999). Only MR 766 infection was reduced by incubation in solutions with higher concentrations of HEPES buffer (Supp. Figure 1C). Furthermore, HEPES buffer concentration only impacted MR 766 infection at concentrations present well after the observed point of pH-induced virus inactivation.

To confirm that ZIKV is endocytosed before release into the cytoplasm, we utilized the fluorophore octadecyl rhodamine B (R18) to identify the location of viral membrane fusion. R18 is a lipophilic, self-quenching fluorophore which can be inserted into viral envelopes at a high enough concentration to quench R18 fluorescence (Loyter et al., 1988; Rinkenberger and Schoggins, 2018). Upon fusion of the labelled viral envelope with another membrane, lipid mixing causes dilution of R18, resulting in fluorescence dequenching. We labelled Asian lineage ZIKV strain PRVABC59 with R18 and infected Huh7.5 cells with labelled virus for 15 min to allow viral entry. We subsequently observed the location of R18 fluorescence relative to the plasma membrane marker wheat germ agglutinin (WGA) with confocal microscopy. As a control, we imaged the colocalization of the plasma membrane marker PM-GFP with WGA. R18 fluorescence was observed predominantly just underneath the plasma membrane (Fig. 1C, Supp. Figure 2A). While plasma membrane localized GFP colocalized with WGA, there was little to no colocalization of R18 fluorescence with WGA (Fig. 1D, Supp. Figure 2B). R18 can undergo nonspecific lipid exchange with adjacent membranes which can result in R18 dequenching in the absence of a membrane fusion event (Stegmann et al., 1993). To confirm that the R18 signal we observed was due to membrane fusion rather than nonspecific lipid exchange, we infected cells with labelled virus in the presence of BafA1 to block endosomal acidifiction, thereby preventing viral fusion. As expected, BafA1 treatment resulted in a dramatic decrease in the amount of R18 dequenching observed (Supp. Fig. 3A and B). These data indicate that ZIKV is released from an internal cell compartment into the cytoplasm.

2.2. African and Asian lineage Zika virus require clathrin-mediated endocytosis and Rab5 function for infection

Next, we compared the dependence of African and Asian lineage ZIKV strains on viral entry-associated host factors and processes known to be important for MR 766 infection. We characterized the effect of siRNA-mediated knockdown of clathrin heavy chain 1 (CLTC), Ras-related C3 botulinum toxin substrate 1 (Rac1), and caveolin-1 (CAV1) on African and Asian lineage ZIKV infection in HeLa cells (Fig. 2A, D, G) (Savidis et al., 2016; Persaud et al., 2018). These host factors are important for clathrin-mediated endocytosis, macropinocytosis, and caveolar endocytosis respectively. We found that infection by all strains of ZIKV was unaffected by Rac1 and CAV1 knockdown. However, CLTC knockdown resulted in a significant reduction in infection irrespective of ZIKV lineage. To validate that gene knockdown impaired endocytic function, we confirmed that clathrin-mediated endocytosis of transferrin was reduced after CLTC knockdown, and that uptake of 70 kDa dextran by macropinocytosis was similarly reduced by Rac1 knockdown (Fig. 2B, E). Reduction in protein expression was confirmed by western blot (Fig. 2C, F, H).

Following endocytosis, enveloped viruses fuse with a specific internal cellular compartment. The most commonly reported site of endocytosed virus fusion is endosomes (Schalich et al., 1996; Daniels

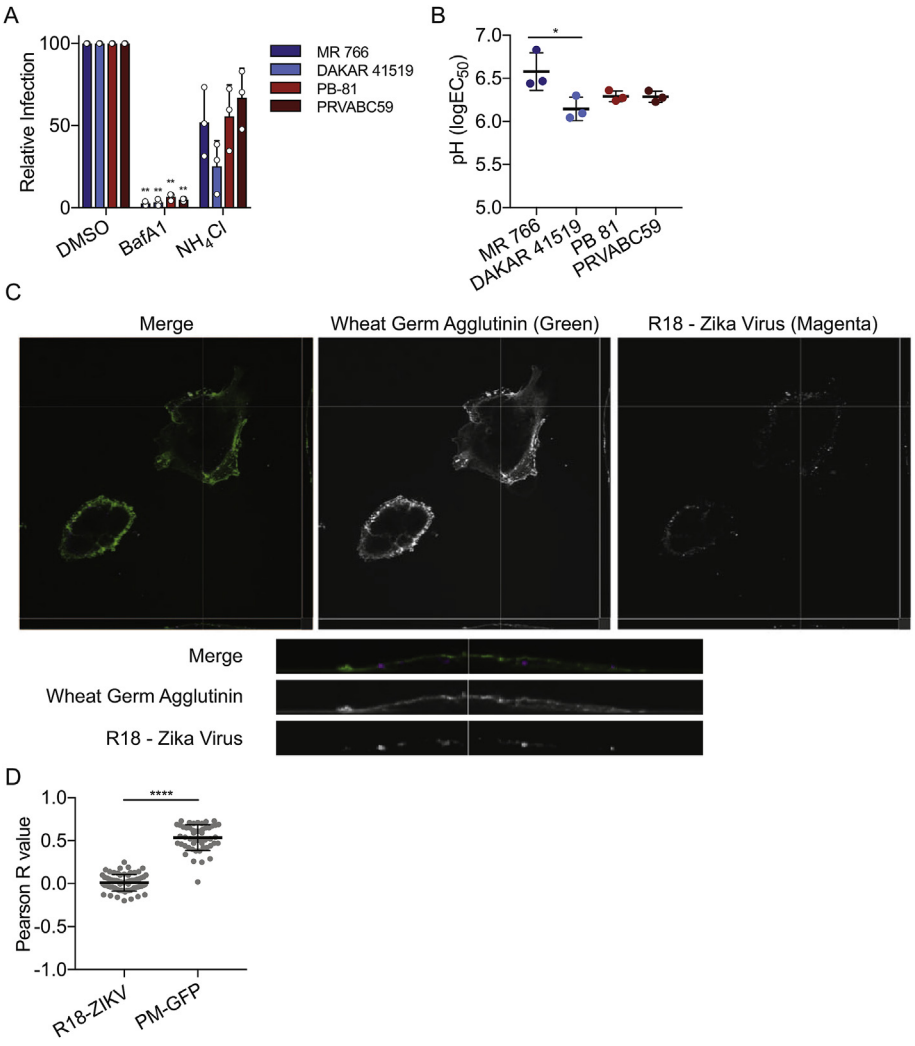

Fig. 1. Zika Virus is Endocytosed During Cell Entry and Enters in a Conserved, pH Dependent Manner. (A) Huh7.5 cells were pretreated with 200 nM BafA1, 10 mM NH_4Cl, or 0.2% DMSO for 1 h and subsequently infected with the ZIKV strains shown in the presence of the above treatments. (B) Indicated ZIKV strains were incubated in buffers between pH 4.4–7.0 for 40 min. The pH of virus-containing buffers was adjusted to pH 7.0 with 1 M pH 8 HEPES and virus inactivation was assessed by infection of Huh7.5 cells. Calculated $logEC_{50}$ values are shown. (C, Top) Huh7.5 cells were infected with R18 labelled PRVABC59 for 15 min, fixed, stained with WGA-AF488, and z-stacks acquired on a confocal microscope. (Bottom) Enlarged z-stack cross sections in the X-Z direction. (D) Pearson correlation coefficients for R18-ZIKV (N = 68) and PM-GFP control (N = 50) colocalization with WGA. Infections were quantitated 24 h post-infection by 4G2 staining and flow cytometry. In A, data represents means of three independent experiments performed in technical triplicate. In B, data represents means of three independent experiments performed in technical singlet or duplicate. In C, representative images from one of three independent experiments are shown. In D, data was collected from three independent experiments. Error bars represent SD. (* $P \leq 0.05$, ** $P \leq 0.01$, **** $P \leq 0.0001$).

et al., 1985; Allison et al., 1995; Korte et al., 1999). Rab5 is important for early endosome function and homotypic fusion (Schalich et al., 1996; Daniels et al., 1985; Allison et al., 1995; Korte et al., 1999). Rab7 is important for endosomal maturation and lysosomal function as well as late endosomal homotypic fusion and fusion with lysosomes (Huotari and Helenius). It was previously shown that expression of a dominant negative mutant variant of Rab5a reduced infection of one ZIKV strain while a dominant negative mutant variant of Rab7a did not (Meertens et al., 2017). To compare the dependency of African and Asian lineage ZIKV infection on Rab5 and Rab7, we expressed the commonly used dominant negative constructs Rab5a S34N and Rab7a N125I in Huh7.5 cells (Fig. 3A). Compared to the control vector, expression of Rab5a S34N but not Rab7a N125I resulted in significantly reduced infection by all ZIKV strains tested. To corroborate these findings, we targeted all *RAB5* and *RAB7* isoforms with CRISPR/Cas9 mediated gene editing. Ablation of Rab5 expression resulted in a similar reduction in infection by all strains of ZIKV tested (Fig. 3B and C). Reduction in Rab7 expression resulted in a significant impairment of Asian lineage ZIKV infection, but only a modest impairment of African lineage ZIKV infection. The observed difference in phenotype between Rab7 dominant negative expression and knockout is likely due to a greater loss in Rab7 function with CRISPR/Cas9 mediated gene editing. Microtubules have also been found to be important for cell entry of MR 766 (Hackett and Cherry, 2018). We found that treatment of Huh7.5 cells with nocodazole efficiently induced microtubule depolymerization, which resulted in a modest reduction of infection by both ZIKV lineages (Supp. Figure 4, Fig. 3D).

2.3. Zika virus preferentially fuses with late endosomes

Our findings indicate that ZIKV is endocytosed and subsequently released into the cytoplasm from an internal cell compartment. We sought to identify the host compartment(s) from which ZIKV is released into the cytoplasm. Considering the above findings suggesting that ZIKV entry is generally conserved between lineages, we only focused on characterizing the entry of the Asian lineage ZIKV strain PRVABC59 in greater detail. Many endocytosed viruses are released into the cytoplasm after penetration or fusion with early endosomes or with multivesicular bodies (MVBs)/late endosomes. To determine if ZIKV is released from early or MVBs/late endosomes, we created stable Huh7.5 cell lines expressing doxycycline-inducible EGFP-Rab5a or EGFP-Rab7a to fluorescently label early endosomes or MVBs/late endosomes respectively. Doxycycline-induced expression of EGFP-Rab5a or EGFP-Rab7a did not significantly impact EGFR degradation kinetics suggesting that vesicular trafficking kinetics and lysosome function were unaffected by EGFP-Rab expresssion (Supp. Fig. 5A and B). We then infected these cells with R18-labelled PRVABC59. Colocalization of lipid mixing events with endosomal markers was observed via R18 fluorescence both in real time by confocal microscopy as well as in fixed cells 15 min after infection (Supp. Movie 1–2, Supp. Figure 6, Fig. 4A). Interestingly, in both data sets we found that the majority of lipid mixing events colocalized with EGFP-Rab7a and a minority of lipid mixing events were colocalized with EGFP-Rab5a (Fig. 4B and C). Our data indicates that ZIKV is capable of fusing with both early and late endosomes but is biased towards late endosomes. This may suggest that

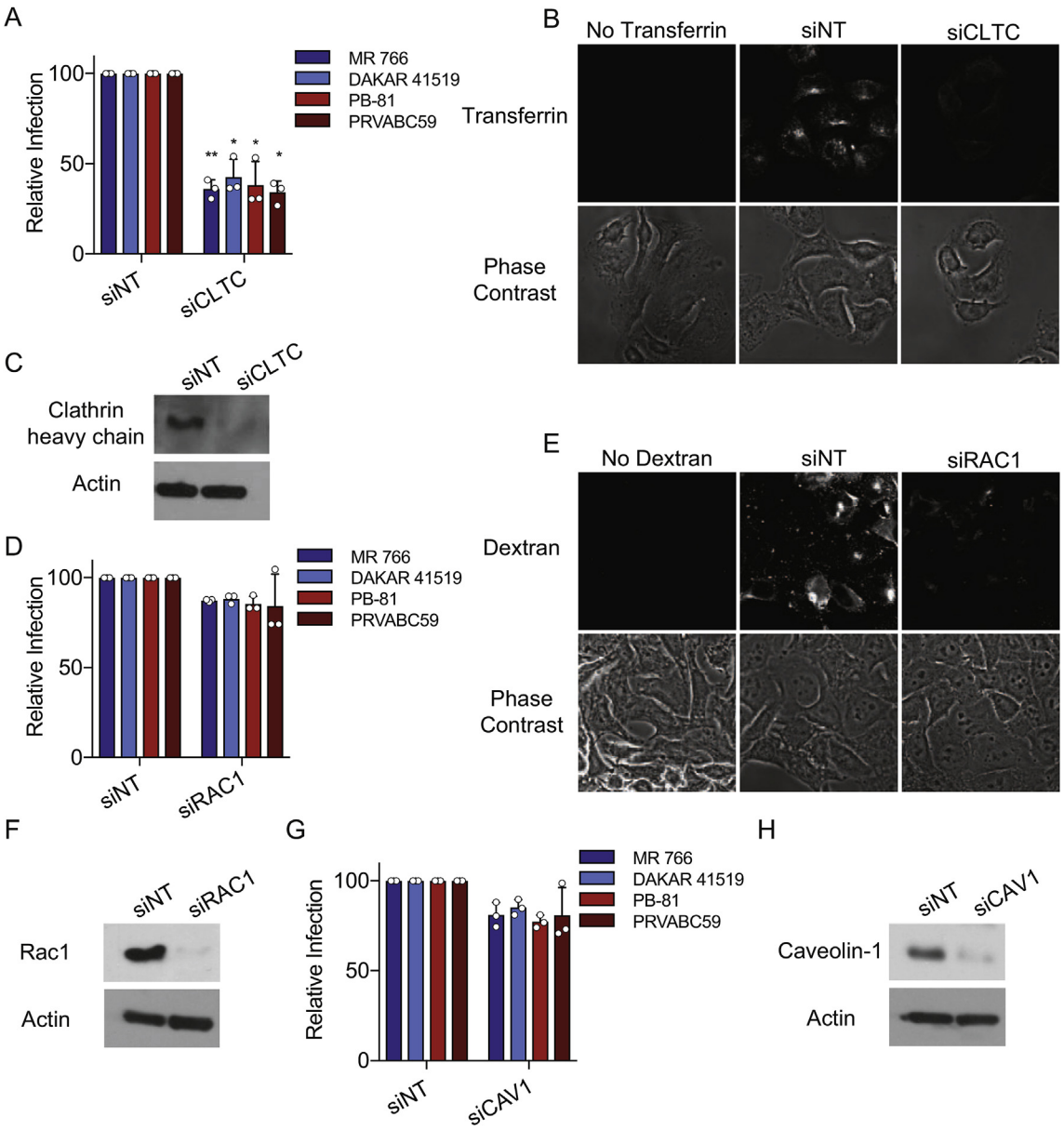

Fig. 2. Asian and African Lineage Zika Virus Require Clathrin for Infection. HeLa cells were transfected with a pool of 3 siRNAs targeting *CLTC* (A–C), *RAC1* (D–F), *CAV1* (G–H), or nontargeting control. (A,D,G) Transfected cells were infected with indicated ZIKV strains. Infection was quantitated 24 h post-infection by 4G2 staining and flow cytometry. (B) Representative confocal images from siRNA transfected Huh7.5 cells serum starved for 1 h and subsequently incubated with or without 25 μg/mL transferrin-AF488 for 20 min. (C) CLTC protein expression levels with indicated siRNA treatment. (E) Representative confocal images from siRNA-transfected Huh7.5 cells that were serum starved for 24 h and subsequently incubated with or without 2 mg/mL 70 kDa FITC-conjugated dextran for 30 min. (F) Rac1 protein expression levels with indicated siRNA treatment. (H) CAV1 protein expression levels with indicated siRNA treatment. In A, D, and G, data represents means of three independent experiments performed in technical triplicate. In all other panels, representative images from at least three independent experiments are shown. Error bars represent SD. (*$P \leq 0.05$, **$P \leq 0.01$).

ZIKV escapes from endosomes as they are maturing from early to MVBs/late endosomes. The GFP-Rab experiments corroborate our dominant negative and knockout data that indicate that Rab5 is necessary for optimal ZIKV infection while Rab7 perturbation has a milder impact on ZIKV infection (Fig. 3). Additionally, the pH range of early endosomes is 6.8–6.2. This decreases to pH 6.2–5.0 in MVBs/late endosomes during endosomal maturation (Jovic et al., 2010; Scott et al., 2014; Hu et al., 2015). Our findings indicate that all tested ZIKV strains except for MR766 are highly sensitive to pH 6.3–6.1. This further suggests that ZIKV fuses with endosomes as they are maturing into MVBs/late endosomes.

Supplementary data related to this article can be found online at https://doi.org/10.1016/j.virol.2019.04.008.

3. Discussion

ZIKV is an emerging pathogen of worldwide concern due to the severe neurological disorders associated with infection (Jovic et al., 2010; Scott et al., 2014; Hu et al., 2015). Understanding the mechanisms underlying ZIKV infection and associated neurological disorders is thus of paramount importance. While at least two lineages of ZIKV exist, only ZIKV strains originating from Asian lineage ZIKV have been associated with significant disease in humans (Zhu et al., 2016; Enfissi et al., 2016; Lanciotti et al., 2016; Haddow et al., 2012; Faye et al., 2014). Thus, studying the differences between ZIKV lineages may help to uncover important elements of ZIKV pathogenesis. During viral infection, the first challenge that a virus must overcome is gaining access

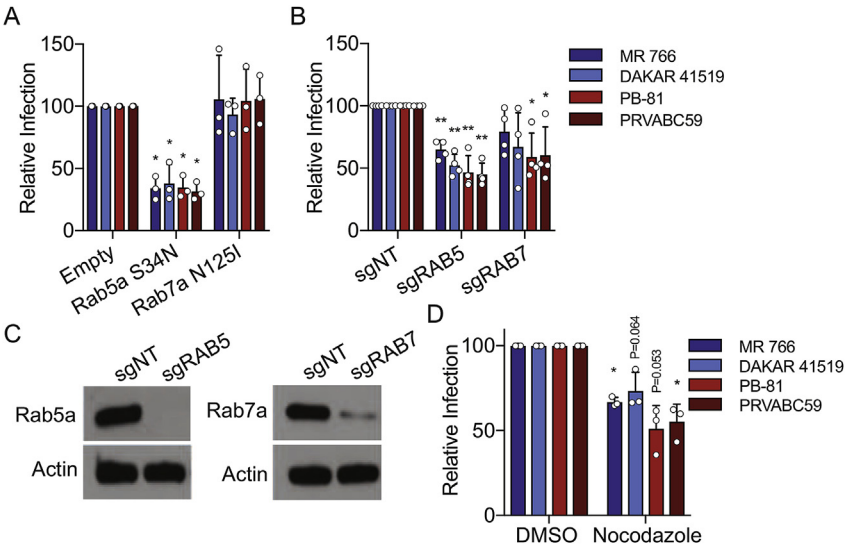

Fig. 3. Asian and African Lineage Zika Virus Require Rab5 for Infection. (A) Huh7.5 cells expressing indicated constructs were infected with the ZIKV strains shown. (B) *RAB5* and *RAB7* loci were targeted with the CRISPR/Cas9 gene editing system in Huh7.5 cells. Cells were subsequently infected with the ZIKV strains shown. (C) Rab5 or Rab7 protein expression after indicated CRISPR/Cas9 mediated gene editing. (D) Huh7.5 cells pretreated with indicated drugs were infected with the ZIKV strains shown. Infections were quantitated 24 h post-infection by 4G2 staining and flow cytometry. In A, B, and D, data represents means of three or four independent experiments performed in technical triplicate. In C, representative images from at least three independent experiments are shown. Error bars represent SD. (*$P \leq 0.05$, **$P \leq 0.01$).

to the host cell cytoplasm. Previous studies suggest that the African lineage of ZIKV is endocytosed via clathrin-mediated endocytosis and fuses with an internal cellular membrane in a Rab5 and pH dependent manner (Meertens et al., 2017; Savidis et al., 2016; Persaud et al., 2018; Rawle et al., 2018). However, previously published studies comparing African and Asian strains identified significant differences in structural protein function and neurovirulence that were associated with lineage-specific mutations in structural genes (Yuan et al., 2017; Bos et al., 2018). While it has been suggested that viral attachment to cells is significantly different between ZIKV lineages, we have found that the general process of ZIKV entry is conserved (Fig. 5) (Bos et al., 2018), and largely mirrors the entry of the flavivirus dengue virus (van der Schaar et al., 2007, 2008a). The infection of multiple African and Asian lineage ZIKV strains that we tested was dependent on functional clathrin-mediated endocytosis, endosomal acidification, and Rab-dependent endosomal trafficking. Additionally, we found that all ZIKV strains tested except for MR 766 are sensitive to pH in the range of 6.1–6.3. This suggests that pH-induced fusion peptide exposure occurs optimally in this pH range. Thus, fusion is likely triggered in strongly acidified early endosomes or recently formed late endosomes. In agreement with this, we showed that ZIKV can fuse at lower frequency with early endosomes but preferentially fuses with MVBs/late endosomes to enter

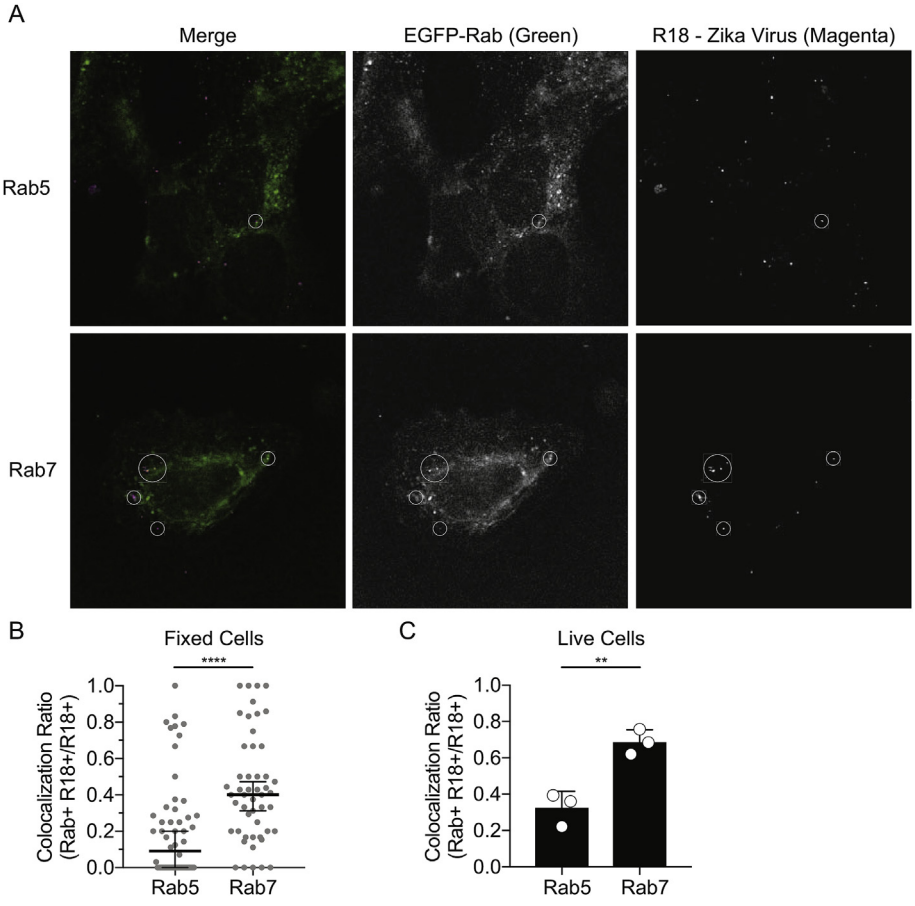

Fig. 4. Zika Virus Fuses Preferentially with Late Endosomes. (A–B) Huh7.5 cells expressing doxycycline-inducible EGFP-Rab5a or EGFP-Rab7a were infected with R18-labelled PRVABC59 for 15 min. (A) Cells were fixed and imaged with confocal microscopy. (B) The ratio of colocalizing R18/EGFP-Rab puncta to the total number of R18 puncta per cell was quantitated for Rab5 (N = 56) and Rab7 (N = 50). (C) Huh7.5 cells expressing doxycycline-inducible EGFP-Rab5a or EGFP-Rab7a were infected with R18-labelled PRVABC59 and imaged in real time with confocal microscopy. The ratio of colocalizing R18/EGFP-Rab puncta to the total number of R18 puncta per experiment was quantitated for Rab5 and Rab7. In A, representative images from three independent experiments are shown. In B, data was collected from three independent experiments. In C, data points represent three independent experiments with N ≥ 25 for each data point. Error bars represent SD. (**$P \leq 0.01$, ****$P \leq 0.0001$).

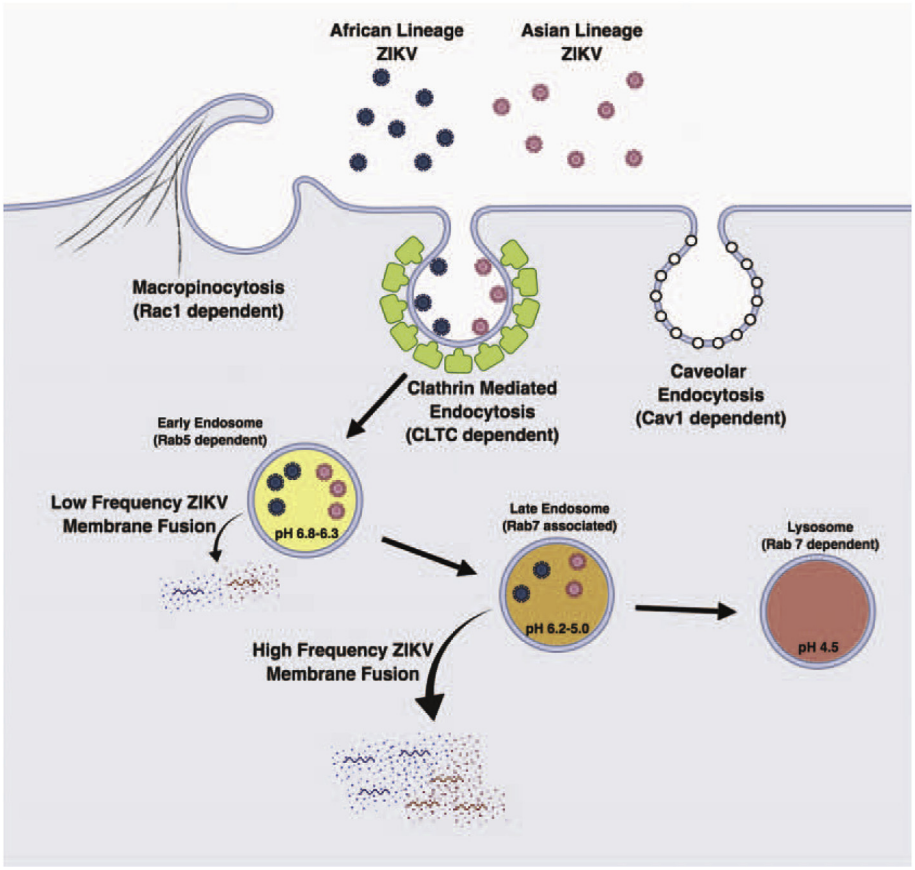

Fig. 5. Model of Zika Virus Entry: ZIKV entry is highly conserved between African and Asian lineages. Following cell surface attachment, ZIKV enters cells through clathrin-mediated endocytosis. Endocytic vesicles containing ZIKV are targeted to the mildly acidic early endosome compartment where the viral envelope fuses with the endosomal membrane at a lower frequency. For the majority of entry events, ZIKV-containing endosomes mature to moderately acidic MVBs and late endosomes, where the viral envelope fuses with the endosomal membrane at a higher frequency. Imaged created with BioRender.

the cytoplasm. In addition to pH, the related flavivirus dengue virus is known to require late endosome associated lipids for efficient fusion (Zaitseva et al., 2010). Accordingly, it is possible that lipid composition in addition to pH may similarly factor into the observed preference of Zika virus to fuse in late endosomes.

The largest difference we observed between ZIKV strains was in the pH sensitivity of the African lineage ZIKV strains MR 766 and DAKAR 41519 (Fig. 1B). While not significant, MR 766 was also inactivated at a higher pH than either Asian lineage strain tested. MR 766 has been passaged over 100 times in tissue culture, and may have adapted distinct entry mechanisms (Helenius, 2018). Consistent with this, our data suggests that the cell entry process of MR 766 may not be fully representative of other ZIKV strains. Additional studies are needed to determine if the increased pH sensitivity of MR 766 significantly affects viral fusion.

While the results presented here suggest that ZIKV enters cells via clathrin-mediated endocytosis, it is intriguing to consider the possibility that ZIKV might infect neurons through a different pathway. Indeed, the infection of another neurovirulent flavivirus, Japanese encephalitis virus (JEV), has been found to be dependent on clathrin-mediated endocytosis in Vero and PK15 kidney-derived epithelial cell lines (Nawa et al., 2003; Yang et al., 2013). However, in neurons, JEV is endocytosed via caveolar endocytosis or macropinocytosis-like processes (Kalia et al., 2013a, 2013b; Zhu et al., 2012). While ZIKV entry mechanisms may also be cell-type dependent, a previous study found that infection of the human microglia-derived cell line CHME3 by a single ZIKV strain required clathrin and Rab5 function (Meertens et al., 2017), similar to our findings. Additional studies are needed to delineate and compare the pathways utilized by African and Asian lineage ZIKV to enter neurons.

Together, our findings suggest that while individual lineages of ZIKV may be capable of using distinct processes to attach to cells, entry into cells is a rather inelastic process (Bos et al., 2018). Our findings further suggest that ZIKV entry is likely not responsible for the observed lineage specific differences *in vitro* or *in vivo*, as this process is conserved between lineages. This could make ZIKV entry a more favorable target for antiviral therapeutics due to its conserved nature.

4. Methods

4.1. Cell lines and viruses

Huh7.5 human hepatoma, HeLa human adenocarcinoma, and human embryonic kidney-derived 293T cells were grown in DMEM supplemented with 10% FBS and 0.1 mM nonessential amino acids. To induce Rab expression, pTRIPZ.GFP-Rab stably expressing Huh7.5 cells were seeded at 4×10^5 cells/well in 24 well plates in normal growth media supplemented with 1.5 μg/mL doxycycline. Cells were replated for experiments 3 days later in doxycycline free media.

ZIKV strain PRVABC59 was obtained from the CDC (GenBank Accession #KU501215). The virus had been passaged three times in Vero cells prior to our acquisition. ZIKV strains DAKAR 41519 and PB-81 were kindly provided by Dr. Kenneth Plante, director of the World Reference Center for Emerging Viruses and Arboviruses. ZIKV strain MR 766 was purchased from ATCC. Virus was propagated no more than 6 total passages for PRVABC59, 3 total passages for PB-81, and 3 total passages for DAKAR 41519. MR 766 has been passaged over 100 times in tissue culture. Viral stocks were prepared by infecting Vero-E6 cells with 0.01–0.05 MOI ZIKV. Cell supernatant was collected 4 days post-infection for MR 766 and 6 days post-infection for all other viruses. Cell supernatant was clarified by centrifugation at $2000 \times g$ for 20 min to remove cellular debris. Virus stocks were stored at −80 °C until use.

4.2. Plasmids and cloning

The lentiviral vector pTRIP.EGFP-PM (gift from C. Rice) expresses

EGFP with a 20 amino acid plasma membrane-targeting farnesylation signal from HRAS fused to the C-terminus (Hancock et al., 1991). The pSCRPSY control construct was prepared as previously described (Schoggins et al., 2011). A plasmid containing the WT Rab5a open reading frame was kindly provided by Dr. Neal Alto. The Rab5a S34N mutant was generated from WT Rab5a by overlap extension PCR using primer sets listed in Supplementary Table 1. A DNA fragment containing the Rab7a N125I open reading frame was synthesized. Genes were amplified by PCR and cloned into pDONR.221 using BP Clonase (Invitrogen) according to the manufacturer's protocol. Genes were cloned using LR Clonase II (Invitrogen) into the previously described lentiviral vector, SCRPSY-DEST, which is puromycin selectable and co-expressed TagRFP (Evrogen) with a gene of interest (Schoggins et al., 2012). For CRISPR/Cas9 experiments, pLentiCRISPRv2 plasmids (a gift from Feng Zhang, Addgene plasmid # 52961) containing Rab targeting guides were kindly provided by Dr. Neal Alto (see Supplementary Table 1). The N-terminally linked GFP-Rab5a open reading frame was PCR amplified with indicated primers (Supplementary Table 1). A DNA fragment containing the N-terminally linked GFP-Rab7a open reading frame was synthesized. The doxycycline-inducible pTRIPZ.GFP-Rab constructs were produced by digesting pTRIPZ (Dharmacon) and above GFP-Rab inserts with AgeI and MluI (NEB) followed by ligation with T4 DNA ligase (NEB).

4.3. Lentivirus production and transduction

SCRPSY lentiviruses were produced as previously described (Schoggins et al., 2012). For lentiCRISPRv2 and TRIPZ.RAB lentivirus production, 293T cells were seeded at 4×10^5 cells per well into 6-well plates. The next day, cells were transfected with 1 μg lentiCRISPRv2, 0.2 μg plasmid expressing VSVg, and 0.8 μg plasmid expressing HIV-1 gag-pol using X-tremeGENE 9 (Roche). Media was changed 6 h later and lentivirus-containing culture supernatants were collected at 48 and 72 h post-transfection. Pooled supernatants were clarified by centrifugation at 800 × *g* for 5 min. HEPES was added to a final concentration of 25 mM. Lentivirus was stored at −80 °C until use.

Cells were seeded at 7×10^4 cells per well in 24 well plates. Media was changed to DMEM supplemented with 4 μg/mL polybrene, 3% FBS, and 25 mM HEPES the next day. Cells were transduced by spinoculation at 800 × *g*, 45 min, 37 °C. Media was changed 6 h later to 10% FBS DMEM supplemented with 0.1 mM nonessential amino acids. For Rab dominant negative experiments, cells were replated at 48 h post-transduction for subsequent experimentation. For Rab CRISPR/Cas9 targeting and TRIPZ.Rab stable cell line generation, cells were selected in 4 μg/mL puromycin for 10–12 days before subsequent experimentation.

4.4. Viral infections

Cells were seeded at 1×10^5 cells per well in 24 well plates 24 h prior to infection. Cells were infected at a MOI of 2.5 with virus diluted in 200 μL (total volume) DMEM containing 1% FBS for 1 h at 37 °C. Afterwards, 500 μL normal growth medium was added to each well. After 24 h, approximately one viral life cycle, cells were dislodged with Accumax, centrifuged at 800 × *g* for 2 min at 4 °C, fixed in 1% PFA for 10 min, and resuspended in PBS with 3% FBS for antibody staining and flow cytometry analysis (Hanners et al., 2016).

4.5. pH inactivation experiments

Huh7.5 cells were seeded at 1×10^5 cells per well in 24 well plates 24 h prior to infection. Phosphate-acetate buffer solutions consisted of 0.9 mM $CaCl_2$, 2.6 mM KCl, 0.5 mM $MgCl_2$, 10 mM K_2HPO_4, and 50 mM acetic acid. Buffer solutions were titrated in 0.2 pH unit increments between pH 4.4 and 7.0 with 5 M NaOH. NaCl was added to each solution to bring the final NaCl concentration to 73.5 mM. The pH of 900 μL of each of the above buffers was or was not changed to pH 7 by addition of 1 M, pH 8.2 HEPES buffer. 1% FBS was added to all solutions. ZIKV strains, diluted to 100 μL in DMEM, were added to each buffer or neutralized control for 40 min at 37 °C. Solution pH after addition of 100 μL DMEM was determined and the adjusted pH was used for the analysis of the experiment. ZIKV containing solutions were adjusted to pH 7 by addition of 1 M, pH 8.2 HEPES buffer. Huh7.5 cells above were infected with 500 μL of the above solutions for 2 h at 37 °C. Media was subsequently changed to 500 μL normal growth media. Infection was quantitated 24 h later by flow cytometry. The best-fit asymmetric 5 parameter curve and corresponding $\log EC_{50}$ value was determined for each data set using Prism 7.

4.6. Drug treatments

Cells were treated with 2.5 μM nocodazole, 200 nM Bafilomycin A1, 10 mM NH_4Cl, or 0.1% DMSO in DMEM containing 1% FBS at 37 °C for 1 h before cell infection. Respective drugs were added to infection media as well as the normal growth media added to each well after infection.

4.7. ZIKV R18 labelling and infection

PRVABC59 was concentrated with ultracentrifugation through a 20% sucrose cushion in an SW-28 rotor at 110,000 × *g* for 90 min. PRVABC59 was diluted to 100 μg/mL viral protein. 6 μL of a 1 mM octadecyl rhodamine B (R18) stock in EtOH was added per mL of ZIKV for 2 h at room temperature. The labelling reaction was filtered through a 0.22 μm filter to remove excess R18. For infections, Huh7.5 cells were seeded at 1×10^5 cells/well in 8 well chamber slides or 35 mm glass bottom dishes (MatTek) the day before infection for fixed or live cell experiments respectively. For the fixed cell data sets, cells were chilled to 4 °C for 30 min. Labelled PRVABC59 was bound to cells at a MOI of 1 in 200 μL DMEM containing 1% FBS for 1 h at 4 °C. Media was subsequently changed to 300 μL DMEM containing 1% FBS warmed to 37 °C. After 15 min, 100 μL 4% PFA was added. For WGA colocalization experiments, cells were then stained with 2 μg/mL Alexa Fluor 488 conjugated WGA (ThermoFisher) for 10 min. Cells were washed twice with PBS containing Ca^{2+}/Mg^{2+} and fixed again with 1% PFA. Alternatively, uninfected Huh7.5 cells stably expressing TRIP.PM-GFP were stained with Alexa Fluor 647 conjugated WGA (ThermoFisher) as above. Slides were mounted with Prolong Gold Antifade Mountant. Rab-R18 colocalization images for fixed cells were taken on a Zeiss LSM 780 confocal microscope. WGA-R18 colocalization z-stacks were taken on an FV10i confocal microscope. After image acquisition, colocalization of R18 dequenching events and PM-GFP with WGA was quantitated with CellSense Dimension Software. Acquired z-stacks were deconvoluted using 50 iterations of the constrained iterative approach. The average Pearson correlation coefficient for all images in deconvoluted z-stacks was determined. Due to the limited amount of R18 signal present in acquired images, Pearson correlation coefficients were determined only for image regions with high R18 signal. For the BafA1 control data set, cells were pretreated with 200 nM BafA1 or 0.2% DMSO in DMEM containing 1% FBS for 30 min. Cells were subsequently infected with labelled PRVABC59 in 200 μL DMEM containing 1% FBS and 200 nM BafA1 or 0.2% DMSO for 15 min at 37 °C. Afterwards, media was replaced with 200 μL 4% PFA. Slides were mounted with Prolong Diamond Antifade Mountant and imaged with a Zeiss LSM 780 confocal microscope. For the live cell data set, cells and virus were equilibrated to room temperature (23 °C) for 30 min. Labelled PRVABC59 was added to cells at a MOI of 1 in 500 μL DMEM containing 1% FBS. Due to timing constraints, images were taken on an FV10i confocal microscope starting at 10 min post-infection every 26s with the 5× confocal aperture setting. After image acquisition, R18 dequenching events and their colocalization with Rab markers was quantitated manually.

4.8. Western blot

Samples were run on a 10% polyacrylamide SDS-PAGE gel, transferred onto nitrocellulose membrane, and blocked for 30 min with 5% milk in TBS containing 0.1% Tween-20 (TBS-T). Membranes were probed with one of the following primary antibodies: 1:1000 anti-CLTC (Sigma, C1860), 1:1000 anti-CAV1 (Sigma, C4490) 1:1000 anti-Rac1 (ThermoFisher, PA1-091), 1:3000 anti-actin (abcam, ab6226), or 1:1000 anti-EGFR (Cell Signaling Tech, 4267). For standard experiments, membranes were washed with TBS-T, probed with goat anti-rabbit or goat anti-mouse HRP conjugated antibodies (Pierce), incubated with ECL substrate (Pierce) according to manufacturer's instructions, and exposed to film. For quantitative experiments, membranes were probed with goat anti-mouse or donkey anti-goat IR Dye conjugated antibodies (Licor). Membranes were washed with TBS and signal was detected using a Licor Odyssey system.

4.9. EGFR degradation assay

Huh7.5 cells were plated in 24-well plates at 1×10^5 cells per well with standard growth media the day before. Cells were washed 2 times with PBS and media was changed to DMEM without serum for 4 h. Media was changed to DMEM containing 100 nM cycloheximide with or without 200 ng/mL EGF. At 0, 1, 2, 3, or 4 h later, cells were washed with PBS and lysed in RIPA buffer containing a 1× protease inhibitor (Roche). EGFR levels relative to actin were quantitated by western blot as described above.

4.10. Antibody staining and flow cytometry

For quantitation of ZIKV infections, infected cells were harvested, permeabilized and stained with 1:2500 anti-Flavivirus Group Antigen Antibody (D1-4G2-4-15) using the Cytofix/Cytoperm kit according to the manufacturer's instructions (BD Bioscience). Samples were subsequently stained with Alexa Fluor 488 conjugated goat anti-mouse antibody (Invitrogen) and cell fluorescence quantified by flow cytometry. An S1000 flow cytometer (Stratedigm) was used and data were analyzed using FlowJo (Treestar). On average a minimum of 10,000 cells were counted per condition. For the virus pH inactivation experiments specifically, a minimum of 4000 cells were counted per condition due to cell loss.

4.11. Immunofluorescence

Wash buffer (WB) consisted of 1% BSA, 0.1% Tween-20 in PBS with Ca^{2+}/Mg^{2+}. Samples were permeabilized for 10 min with 0.2% Triton X-100 in WB and blocked overnight in WB. Samples were incubated with 1:1000 anti-α-tubulin (Sigma, T6074) in WB for 1 h, washed 2 times in WB for 1 min each, and probed with 1:1000 goat anti-mouse Alexa Fluor 488 conjugated antibody (Life Technologies) in WB for 1 h. Samples were washed twice with WB. Samples were mounted with Prolong Gold Antifade Mountant (ThermoFisher). Immunofluorescence samples were imaged with epifluorescence microscopy on a Nikon ECLIPSE Ti.

4.12. siRNA mediated knockdown

HeLa cells were seeded at 5×10^4 cells/well in 24 well plates 24 h before siRNA transfection in 500 µL normal growth media. 0.2 µL of 20 µM SMARTpool siRNAs (Dharmacon) targeting *CLTC* (L-004001-01-0005), *RAC1* (L-003560-00-0005), *CAV1* (L-003467-00-0005), or non-targeting control (D-001206-14-05) were diluted in 100 µL DMEM. Subsequently, 3 µL HiPerfect transfection reagent was added. After 10 min, transfection complexes were added to the above cells. 2 days later, cells were replated for experimentation.

4.13. Endocytic marker uptake

HeLa cells were seeded at 2×10^4 cells/well in 8-well chamber slides in normal growth media. The next day, cells were washed once and incubated in serum free DMEM for 1 or 24 h for transferrin or dextran uptake assays respectively. For transferrin uptake, cells were incubated with 25 µg/mL Alexa Fluor 488 conjugated transferrin (ThermoFisher) in DMEM for 20 min. For dextran uptake, cells were incubated with 2 mg/mL FITC conjugated 70 kDa dextran (ThermoFisher) for 30 min. Cells were washed once with DMEM and fixed with 4% PFA for 10 min. Slides were mounted with Prolong Gold Antifade Mountant and imaged with an FV10i confocal microscope.

5. Statistical analysis

For normalized data sets, a ratio paired T test was used to determine statistical significance. For the EGFR degradation experiments, a two-way ANOVA was used. For analysis of $\log EC_{50}$ values generated from the pH inactivation experiment, a one-way analysis of variance (ANOVA) with Sidak's post-test was used. For all other data sets, statistical significance was determined using a Student's T test with Welch's correction.

Acknowledgements

We thank Jennifer Eitson and Didi Chen for technical assistance, and Katrina Mar for critical manuscript feedback. We acknowledge the assistance of the UT Southwestern Live Cell Imaging Facility, a shared resource of the Harold C. Simmons Cancer Center, supported in part by an NCI Cancer Center Support Grant, CA142543. This work was supported in part by NIH grants AI117922 and by the UT Southwestern Endowed Scholars program (J.W.S.). Additional support for N.R. was obtained from NIH T32 Training Grant AI007520.

Appendix A. Supplementary data

Supplementary data to this article can be found online at https://doi.org/10.1016/j.virol.2019.04.008.

References

Allison, S.L., Schalich, J., Stiasny, K., Mandl, C.W., Kunz, C., Heinz, F.X., 1995. Oligomeric rearrangement of tick-borne encephalitis virus envelope proteins induced by an acidic pH. J. Virol. 69, 695.

Anfasa, F., Siegers, J.Y., van der Kroeg, M., Mumtaz, N., Stalin Raj, V., de Vrij, F.M.S., Widagdo, W., Gabriel, G., Salinas, S., Simonin, Y., Reusken, C., Kushner, S.A., Koopmans, M.P.G., Haagmans, B., Martina, B.E.E., van Riel, D., 2017. Phenotypic differences between Asian and African lineage Zika viruses in human neural progenitor cells. mSphere 2 e00292-17.

Beaver, J.T., Lelutiu, N., Habib, R., Skountzou, I., 2018. Evolution of two major Zika virus lineages: implications for pathology, immune response, and vaccine development. Front. Immunol. 9, 1640 1640.

Bos, S., Viranaicken, W., Turpin, J., El-Kalamouni, C., Roche, M., Krejbich-Trotot, P., Despres, P., Gadea, G., 2018. The structural proteins of epidemic and historical strains of Zika virus differ in their ability to initiate viral infection in human host cells. Virology 516, 265–273.

Chu, J.J.H., Ng, M.L., 2004. Infectious entry of west nile virus occurs through a clathrin-mediated endocytic pathway. J. Virol. 78, 10543.

Daniels, R.S., Downie, J.C., Hay, A.J., Knossow, M., Skehel, J.J., Wang, M.L., Wiley, D.C., 1985. Fusion mutants of the influenza virus hemagglutinin glycoprotein. Cell 40, 431–439.

Enfissi, A., Codrington, J., Roosblad, J., Kazanji, M., Rousset, D., 2016. Zika virus genome from the Americas. Lancet 387, 227–228.

Faria, N.R., Azevedo, RdSdS., Kraemer, M.U.G., Souza, R., Cunha, M.S., Hill, S.C., Thézé, J., Bonsall, M.B., Bowden, T.A., Rissanen, I., Rocco, I.M., Nogueira, J.S., Maeda, A.Y., Vasami, FGdS., Macedo, FLdL., Suzuki, A., Rodrigues, S.G., Cruz, A.C.R., Nunes, B.T., Medeiros, DBdA., Rodrigues, D.S.G., Queiroz, A.L.N., da Silva, E.V.P., Henriques, D.F., da Rosa, E.S.T., de Oliveira, C.S., Martins, L.C., Vasconcelos, H.B., Casseb, L.M.N., Simith, DdB., Messina, J.P., Abade, L., Lourenço, J., Alcantara, L.C.J., de Lima, M.M., Giovanetti, M., Hay, S.I., de Oliveira, R.S., Lemos, PdS., de Oliveira, L.F., de Lima, C.P.S., da Silva, S.P., de Vasconcelos, J.M., Franco, L., Cardoso, J.F., Vianez-Júnior, JLdSG., Mir, D., Bello, G., Delatorre, E., Khan, K., et al., 2016. Zika virus in the Americas: early epidemiological and genetic findings. Science (New York, NY)

352, 345–349.
Faye, O., Freire, C.C.M., Iamarino, A., Faye, O., de Oliveira, J.V.C., Diallo, M., Zanotto, P.M.A., Sall, A.A., 2014. Molecular evolution of Zika virus during its emergence in the 20(th) century. PLoS Neglected Trop. Dis. 8, e2636 e2636.
Hackett, B.A., Cherry, S., 2018. Flavivirus internalization is regulated by a size-dependent endocytic pathway. Proc. Natl. Acad. Sci. Unit. States Am. 115, 4246.
Haddow, A.D., Schuh, A.J., Yasuda, C.Y., Kasper, M.R., Heang, V., Huy, R., Guzman, H., Tesh, R.B., Weaver, S.C., 2012. Genetic characterization of Zika virus strains: geographic expansion of the Asian lineage. PLoS Neglected Trop. Dis. 6, e1477.
Hancock, J.F., Cadwallader, K., Paterson, H., Marshall, C.J., 1991. A CAAX or a CAAL motif and a second signal are sufficient for plasma membrane targeting of ras proteins. EMBO J. 10, 4033–4039.
Hanners, N.W., Eitson, J.L., Usui, N., Richardson, R.B., Wexler, E.M., Konopka, G., Schoggins, J.W., 2016. Western Zika virus in human fetal neural progenitors persists long term with partial cytopathic and limited immunogenic effects. Cell Rep. 15, 2315–2322.
Helenius, A., 2018. Virus entry: looking back and moving forward. J. Mol. Biol. 430, 1853–1862.
Helenius, A., Kartenbeck, J., Simons, K., Fries, E., 1980. On the entry of Semliki forest virus into BHK-21 cells. J. Cell Biol. 84, 404–420.
Hills, S.L., Fischer, M., Petersen, L.R., 2017. Epidemiology of Zika virus infection. J. Infect. Dis. 216, S868–S874.
Hu, Y.-B., Dammer, E.B., Ren, R.-J., Wang, G., 2015. The endosomal-lysosomal system: from acidification and cargo sorting to neurodegeneration. Transl. Neurodegener. 4, 18 18.
Huotari J, Helenius A. Endosome maturation. EMBO J. 30:3481-3500.
Jovic, M., Sharma, M., Rahajeng, J., Caplan, S., 2010. The early endosome: a busy sorting station for proteins at the crossroads. Histol. Histopathol. 25, 99–112.
Kalia, M., Khasa, R., Sharma, M., Nain, M., Vrati, S., 2013a. Japanese encephalitis virus infects neuronal cells through a clathrin-independent endocytic mechanism. J. Virol. 87, 148–162.
Kalia, M., Khasa, R., Sharma, M., Nain, M., Vrati, S., 2013b. Japanese encephalitis virus infects neuronal cells through a clathrin-independent endocytic mechanism. J. Virol. 87, 148.
Korte, T., Ludwig, K., Booy, F.P., Blumenthal, R., Herrmann, A., 1999. Conformational intermediates and fusion activity of influenza virus hemagglutinin. J. Virol. 73, 4567.
Lanciotti, R.S., Lambert, A.J., Holodniy, M., Saavedra, S., Signor, L.D.C.C., 2016. Phylogeny of Zika virus in western hemisphere, 2015. Emerg. Infect. Dis. 22, 933–935.
Laureti, M., Narayanan, D., Rodriguez-Andres, J., Fazakerley, J.K., Kedzierski, L., 2018. Flavivirus receptors: diversity, identity, and cell entry. Front. Immunol. 9, 2180 2180.
Lazear, H.M., Govero, J., Smith, A.M., Platt, D.J., Fernandez, E., Miner, J.J., Diamond, M.S., 2016. A mouse model of Zika virus pathogenesis. Cell Host Microbe 19, 720–730.
Loyter, A., Citovsky, V., Blumenthal, R., 1988. The use of fluorescence dequenching measurements to follow viral membrane fusion events. Methods Biochem. Anal. 33, 129–164 Review. PubMed PMID: 3128721.
Meertens, L., Labeau, A., Dejarnac, O., Cipriani, S., Sinigaglia, L., Bonnet-Madin, L., Le Charpentier, T., Hafirassou, M.L., Zamborlini, A., Cao-Lormeau, V.M., Coulpier, M., Misse, D., Jouvenet, N., Tabibiazar, R., Gressens, P., Schwartz, O., Amara, A., 2017. Axl mediates Zika virus entry in human glial cells and modulates innate immune responses. Cell Rep 18, 324–333.
Muller, J.A., Harms, M., Schubert, A., Jansen, S., Michel, D., Mertens, T., Schmidt-Chanasit, J., Munch, J., 2016. Inactivation and environmental stability of Zika virus. Emerg. Infect. Dis. 22, 1685–1687.
Nawa, M., Takasaki, T., Yamada, K., Kurane, I., Akatsuka, T., 2003. Interference in Japanese encephalitis virus infection of Vero cells by a cationic amphiphilic drug, chlorpromazine. J. Gen. Virol. 84, 1737–1741.
Persaud, M., Martinez-Lopez, A., Buffone, C., Porcelli, S.A., Diaz-Griffero, F., 2018. Infection by Zika viruses requires the transmembrane protein AXL, endocytosis and low pH. Virology 518, 301–312.
Rawle, R.J., Webster, E.R., Jelen, M., Kasson, P.M., Boxer, S.G., 2018. pH dependence of Zika membrane fusion kinetics reveals an off-pathway state. ACS Cent. Sci. 4, 1503–1510.
Rinkenberger, N., Schoggins, J.W., 2018 Jan 30. Mucolipin-2 cation channel increases trafficking efficiency of endocytosed viruses. MBio 9 (1) PII: e02314-17. DOI: 10.1128/mBio.02314-17. PubMed PMID: 29382735; PubMed Central PMCID: PMC5790917.
Sánchez-San Martín, C., Liu, C.Y., Kielian, M., 2009. Dealing with low pH: entry and exit of alphaviruses and flaviviruses. Trends Microbiol. 17, 514–521.
Savidis, G., McDougall, W.M., Meraner, P., Perreira, J.M., Portmann, J.M., Trincucci, G., John, S.P., Aker, A.M., Renzette, N., Robbins, D.R., Guo, Z., Green, S., Kowalik, T.F., Brass, A.L., 2016. Identification of Zika virus and dengue virus dependency factors using functional genomics. Cell Rep 16, 232–246.
Schalich, J., Allison, S.L., Stiasny, K., Mandl, C.W., Kunz, C., Heinz, F.X., 1996. Recombinant subviral particles from tick-borne encephalitis virus are fusogenic and provide a model system for studying flavivirus envelope glycoprotein functions. J. Virol. 70, 4549.
Schoggins, J.W., Wilson, S.J., Panis, M., Murphy, M.Y., Jones, C.T., Bieniasz, P., Rice, C.M., 2011. A diverse range of gene products are effectors of the type I interferon antiviral response. Nature 472, 481–485.
Schoggins, J.W., Dorner, M., Feulner, M., Imanaka, N., Murphy, M.Y., Ploss, A., Rice, C.M., 2012. Dengue reporter viruses reveal viral dynamics in interferon receptor-deficient mice and sensitivity to interferon effectors in vitro. Proc. Natl. Acad. Sci. U. S. A. 109, 14610–14615.
Scott, C.C., Vacca, F., Gruenberg, J., 2014. Endosome maturation, transport and functions. Semin. Cell Dev. Biol. 31, 2–10.
Simonin, Y., Loustalot, F., Desmetz, C., Foulongne, V., Constant, O., Fournier-Wirth, C., Leon, F., Moles, J.P., Goubaud, A., Lemaitre, J.M., Maquart, M., Leparc-Goffart, I., Briant, L., Nagot, N., Van de Perre, P., Salinas, S., 2016. Zika virus strains potentially display different infectious profiles in human neural cells. EBioMedicine 12, 161–169.
Smith, D.R., Sprague, T.R., Hollidge, B.S., Valdez, S.M., Padilla, S.L., Bellanca, S.A., Golden, J.W., Coyne, S.R., Kulesh, D.A., Miller, L.J., Haddow, A.D., Koehler, J.W., Gromowski, G.D., Jarman, R.G., Alera, M.T.P., Yoon, I.K., Buathong, R., Lowen, R.G., Kane, C.D., Minogue, T.D., Bavari, S., Tesh, R.B., Weaver, S.C., Linthicum, K.J., Pitt, M.L., Nasar, F., 2018. African and Asian Zika virus isolates display phenotypic differences both in vitro and in vivo. Am. J. Trop. Med. Hyg. 98, 432–444.
Stauffer, S., Feng, Y., Nebioglu, F., Heilig, R., Picotti, P., Helenius, A., 2014. Stepwise priming by acidic pH and a high K^+ concentration is required for efficient uncoating of influenza a virus cores after penetration. J. Virol. 88, 13029.
Stegmann, T., Schoen, P., Bron, R., Wey, J., Bartoldus, I., Ortiz, A., Nieva, J.L., Wilschut, J., 1993. Evaluation of viral membrane fusion assays. Comparison of the octadecylrhodamine dequenching assay with the pyrene excimer assay. Biochemistry 32, 11330–11337.
Stiasny, K., Fritz, R., Pangerl, K., Heinz, F.X., 2011. Molecular mechanisms of flavivirus membrane fusion. Amino Acids 41, 1159–1163.
van der Schaar, H.M., Rust, M.J., Waarts, B.-L., van der Ende-Metselaar, H., Kuhn, R.J., Wilschut, J., Zhuang, X., Smit, J.M., 2007. Characterization of the early events in dengue virus cell entry by biochemical assays and single-virus tracking. J. Virol. 81, 12019.
van der Schaar, H.M., Rust, M.J., Chen, C., van der Ende-Metselaar, H., Wilschut, J., Zhuang, X., Smit, J.M., 2008a. Dissecting the cell entry pathway of dengue virus by single-particle tracking in living cells. PLoS Pathog 4, e1000244.
van der Schaar, H.M., Rust, M.J., Chen, C., van der Ende-Metselaar, H., Wilschut, J., Zhuang, X., Smit, J.M., 2008b. Dissecting the cell entry pathway of dengue virus by single-particle tracking in living cells. PLoS Pathog. 4, e1000244.
Ventura, C.V., Ventura, L.O., 2018. Ophthalmologic manifestations associated with Zika virus infection. Pediatrics 141, S161–S166.
Wang, L., Valderramos, S.G., Wu, A., Ouyang, S., Li, C., Brasil, P., Bonaldo, M., Coates, T., Nielsen-Saines, K., Jiang, T., Aliyari, R., Cheng, G., 2016. From mosquitos to humans: genetic evolution of Zika virus. Cell Host Microbe 19, 561–565.
White, J.M., Whittaker, G.R., 2016. Fusion of enveloped viruses in endosomes. Traffic 17, 593–614.
Yang, S., He, M., Liu, X., Li, X., Fan, B., Zhao, S., 2013. Japanese encephalitis virus infects porcine kidney epithelial PK15 cells via clathrin- and cholesterol-dependent endocytosis. Virol. J. 10, 258.
Yuan, L., Huang, X.Y., Liu, Z.Y., Zhang, F., Zhu, X.L., Yu, J.Y., Ji, X., Xu, Y.P., Li, G., Li, C., Wang, H.J., Deng, Y.Q., Wu, M., Cheng, M.L., Ye, Q., Xie, D.Y., Li, X.F., Wang, X., Shi, W., Hu, B., Shi, P.Y., Xu, Z., Qin, C.F., 2017. A single mutation in the prM protein of Zika virus contributes to fetal microcephaly. Science 358, 933–936.
Zaitseva, E., Yang, S.T., Melikov, K., Pourmal, S., Chernomordik, L.V., 2010. Dengue virus ensures its fusion in late endosomes using compartment-specific lipids. PLoS Pathog 6, e1001131.
Zhang, F., Hammack, C., Ogden, S.C., Cheng, Y., Lee, E.M., Wen, Z., Qian, X., Nguyen, H.N., Li, Y., Yao, B., Xu, M., Xu, T., Chen, L., Wang, Z., Feng, H., Huang, W.K., Yoon, K.J., Shan, C., Huang, L., Qin, Z., Christian, K.M., Shi, P.Y., Xu, M., Xia, M., Zheng, W., Wu, H., Song, H., Tang, H., Ming, G.L., Jin, P., 2016. Molecular signatures associated with ZIKV exposure in human cortical neural progenitors. Nucleic Acids Res 44, 8610–8620.
Zhu, Y.-Z., Xu, Q.-Q., Wu, D.-G., Ren, H., Zhao, P., Lao, W.-G., Wang, Y., Tao, Q.-Y., Qian, X.-J., Wei, Y.-H., Cao, M.-M., Qi, Z.-T., 2012. Japanese encephalitis virus enters rat neuroblastoma cells via a pH-dependent, dynamin and caveola-mediated endocytosis pathway. J. Virol. 86, 13407–13422.
Zhu, Z., Chan, J.F., Tee, K.M., Choi, G.K., Lau, S.K., Woo, P.C., Tse, H., Yuen, K.Y., 2016. Comparative genomic analysis of pre-epidemic and epidemic Zika virus strains for virological factors potentially associated with the rapidly expanding epidemic. Emerg. Microb. Infect. 5, e22.